Available online at www.sciencedirect.com
ScienceDirect
Thermochimica Acta 464 (2007) 16–23
thermochimica acta
www.elsevier.com/locate/tca

# Dynamic effective thermal properties of ceramics–metal functionally graded fibrous composites

C. Hu [a,b], X.-Q. Fang [b,*]

[a] School of Aerospace Engineering and Mechanics, Tongji University, Shanghai 200092, China
[b] School of Astronautics, P.O. Box 137, Harbin Institute of Technology, Harbin 150001, China

Received 27 March 2007; received in revised form 23 July 2007; accepted 9 August 2007
Available online 15 August 2007

**Abstract**

This work is dedicated to investigate the dynamic effective thermal properties of ceramics–metal functionally graded fibrous composites resulting from thermal waves. A micromechanics-based thermo-dynamical model is developed to predict the distribution of dynamic effective thermal properties of functionally graded fibrous composites in the gradation direction. Generally speaking, in functionally graded materials there exist two microstructurally distinct zones: fiber–matrix zone and a transition zone. In fiber–matrix zone, based on the heat conduction equation in materials, the dynamic effective thermal properties for any macroscopic material points are determined by employing effective medium method in the corresponding microstructural representative volume element (RVE). In transition zone, a transition function is introduced to make the wave fields continuous and differentiable. Numerical examples of the dynamic effective thermal properties in the gradation direction under different parameters are graphically presented. Obtained results reveal that the material properties of each phase, the incident frequency, and the gradation parameter of materials have great effect on the distribution of dynamic effective properties in the gradation direction. In different material zones, the effect displays great difference. At last, the results are discussed in detail.


*Keywords:* Functionally graded materials; Multiple scattering of thermal waves; Effective medium method; Dynamic effective thermal properties

## 1. Introduction

Functionally graded materials (FGMs) are a new generation of engineering materials, wherein the micro-structural details are spatially varied through non-uniform distributions of the reinforcement phases. An ideal FGM combines the best properties of metals and ceramics—the toughness, electrical conductivity, and machinability of metals, and the low density, high strength, high stiffness, and temperature resistance of ceramics. The volume fraction of FGMs changes gradiently, and the non-homogeneous microstructures in the materials produce continuous graded macroscopic properties, such as the thermal conductivity, specific heat, mass density and elastic modulus. All the properties make FGMs preferable in many advanced applications, e.g., thermal barrier coating, thermal protection of reentry capsule, furnace liners, personal body armor, and heat resistance materials for the electromagnetic sensors [1,2]. So the theoretical and experimental investigations of the effective properties of FGMs have received great interest in recent years.

The determination of the static effective properties of functionally graded materials has been reported in some literatures in the past decade. There are many methods that are currently applied for getting the material property distribution of FGMs. The most common method is the law of mixture method, which is normally used for laminated composites. The power law and the exponential law are also commonly used in many researches. Khor and Gu [3] presented an experimental investigation on the thermal diffusivity/conductivity of plasma-sprayed functionally graded thermal barrier coating, and the mixture method of the material properties was considered. By means of essential and natural boundary conditions, Ostoja-Starzewski and Schulte [4] demonstrated the effective thermal conductivities of FGMs. Based on a micromechanics-based elastic model, Yin et al. also derived the static effective elastic properties (Young's modulus and Poisson's ratio) [5] and effective thermal property (thermal

* Corresponding author. Tel.: +86 45186410268.
*E-mail address:* fangxueqian@163.com (X.-Q. Fang).

0040-6031/$ – see front matter © 2007 Elsevier B.V. All rights reserved.
doi:10.1016/j.tca.2007.08.002

conductivity) [6] of functionally graded materials, and the power law variation of material properties was considered.

It is well known that the material structures under dynamic mechanical and thermal loading are more important in engineering [7], so the researches on the dynamic effective properties of composite materials are crucial for designing more practical materials. However, due to the coherence of wave scattering in dynamics and the multiple scattering of thermal waves among the fibers, the theoretical analysis of the dynamic effective properties constitutes a much more difficult task than that of the static problem. Up to present time, the researches on the dynamic effective properties mainly focused on the effective properties under mechanical loading. Based on the multiple scattering theory, Foldy [8] studied earlier the effective wave number of the scalar wave propagating through the inhomogeneous medium with distributed particles. Subsequently, Bose and Mal [9] extended the multiple scattering theory of the scalar waves to the elastic waves and enhanced the theory by introducing the more realistic pair-correlation function to describe the interaction between two particles accurately. Adopting Foldy's theory, Nozaki [10] studied the propagation and scattering of P and SV waves in a fiber-reinforced metal–matrix composite with thick non-homogeneous interface layers and the effect of the layer property on effective elastic modulus was also analyzed. Liu and Kriz [11] investigated the scattering of shear waves in a multiphase fiber–matrix composite, and the effect of interfacial material properties on the dynamic effective properties was also discussed.

To the authors' knowledge, the literatures on the dynamic effective thermal properties of FGMs are limited in numbers. To obtain desired thermal properties and dynamical reliability, reasonable dynamical thermal models are required. Recently, Chakrborty and Gopalakrishnan [12] employed spectral finite element method to analyze the wave propagation behavior in a functionally graded beam subjected to high frequency impulse loading. The thermal and mechanical properties are modeled either by explicit distribution law like the power law and the exponential law or by rule of mixture. A new beam element was also developed to study the thermoelastic behavior of functionally graded beam structures, and both exponential and power law variations of material property distribution were considered [13].

In the present paper, effective medium method (EMM) is applied to predict the dynamic thermal behavior of FGMs under thermal waves. Effective medium method is a more accurate method for evaluating the effective field and computing the dynamic effective properties in randomly distributed elastic medium, and it has been successfully applied to analyze the wave field in composite materials [14,15]. By making use of this method, one can change an original inhomogeneous medium for a homogeneous one with the effective dynamic properties of the former (the homogenization problem). This substitution essentially simplifies the analysis of the propagation of various types of waves in composite materials. The effective medium which is equivalent to the original composite material is a medium with space and time dispersion, and hence, its parameters are functions of frequency of the incident field.

The remainder of this paper is organized as follows. In Section 2, a micromechanics-based thermo-dynamical model is constructed for analyzing the microstructure of fiber-reinforced graded materials. The power law variation of the material properties is considered. In the fiber–matrix zone, a representative volume element (RVE) for a material point is used to statistically represent the microstructure in the neighborhood. In Section 3, based on Fourier heat conduction equation in materials, the dispersion relation of effective wave number in the RVE of zone 1 is derived by using effective medium method, and the dynamic effective thermal properties (thermal conductivity, specific heat capacity and mass density) are obtained by iterative scheme. The dynamic effective thermal properties in zones 2 and 3 are calculated in Section 4. In Section 5, the numerical examples of dynamic effective thermal properties under different parameters are graphically presented. Comparisons with the static effective thermal properties in previous literatures are also presented and discussed. Section 6 presents the detailed conclusion of this investigation.

## 2. A micromechanics-based thermo-dynamic model of temperature field in functionally graded materials

Consider a typical fiber-reinforced FGM microstructure with a gradual compositional variation from heat resistant ceramics to fracture-resistant metals, which is depicted in Fig. 1. The global coordinate system of the FGM is denoted by (XOY) with $Y$ being the continuous gradation direction. The overall gradation thickness of the FGM is $d$. Three material zones exist in the gradation direction: zone 1 ($0 \le Y \le d_1$) including phase $B$ fibers with phase $A$ matrix, zone 3 ($d_2 \le Y \le d$) including phase $A$ fibers with phase $B$ matrix, and the transition zone 2 ($d_1 \le Y \le d_2$). In fiber–matrix zone, it is assumed that the dispersed fibers parallel to each other are distributed randomly in continuous matrix. In the transition zone, the fiber and matrix phases cannot be well

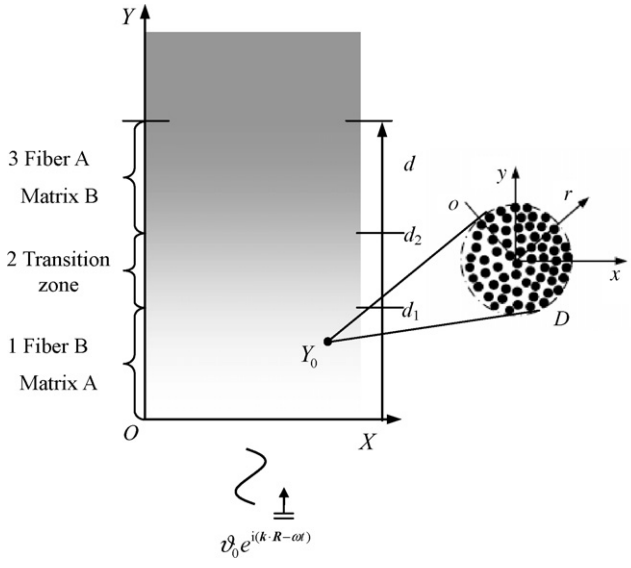


Fig. 1. Schematic of material zones and incident waves in functionally graded materials.

defined because the two phases are interpenetrated into each other as a connected network.

For simplicity, both phases are assumed to be isotropic materials, and in each fiber–matrix zone fibers are assumed to be identical cylinders fully bonded to the matrix. The volume fraction of fibers varies gradually, and the variational function is $\phi(Y) = (Y/d)^m$, in which $m$ is the gradation parameter [6,12,13]. Let $\lambda_A$, $c_A$, $\rho_A$ be the thermal conductivity, specific heat capacity and mass density of phase A, and $\lambda_B$, $c_B$, $\rho_B$ those of phase B. Suppose that a monochromatic thermal wave of frequency $\omega$ propagates in the fiber–matrix FGM along the $Y$ direction.

A microscopic representative volume element (RVE) is proposed to represent the microstructure in the neighborhood of a material point in the fiber–matrix zone. For any macroscopic material point $Y_0$ in the range of $(0 \le Y \le d_1)$, the corresponding micro-structural RVE contains a number of identical fibers of phase B embedded in a continuous matrix of phase A, so that the overall volume fraction of phase B should be consistent with the macroscopic counterparts $\phi(Y_0)$. As seen in Fig. 1, the whole RVE domain is denoted by $D$, and the microscopic coordinate system (oxy) is constructed with its origin at the material point $Y_0$. In the RVE, the effective medium method is employed to derive the dynamic effective thermal properties and wave fields.

## 3. Solution of dynamic effective thermal properties in zone 1

In the two-dimensional case, when the inner thermal source is omitted, the heat conduction equation in materials is expressed as

$$\lambda(r)\nabla^2 T + \nabla\lambda(r)\cdot\nabla T = \rho(r)c(r)\frac{\partial T(r,t)}{\partial t}, \tag{1}$$

where $\nabla$ is the nabla operator, $\nabla^2 = \partial^2/\partial x^2 + \partial^2/\partial y^2$ is the two-dimensional Laplace operator, $T(r,t)$ is the temperature in materials, and $\lambda(r)$, $c(r)$ and $\rho(r)$ are the thermal conductivity, specific heat capacity and density of materials, respectively.

The unsteady and periodical solution of the problem is investigated. Let $T = T_0 + Re[\vartheta(r)\exp(-i\omega t)]$, Eq. (1) can be changed into the following equation [16]:

$$\lambda(r)\nabla^2\vartheta(r) + \nabla\lambda(r)\nabla\vartheta(r) + i\omega\rho(r)c(r)\vartheta(r) = 0, \tag{2}$$

Here $T_0$ is the mean temperature in materials, $\vartheta(r)$ is the amplitude of temperature, $\omega$ is the circular frequency of thermal waves.

Suppose that $\lambda(r)$, $c(r)$ and $\rho(r)$ may be presented as the following sums:

$$\lambda(r) = \lambda_A + \lambda_1 s(r), \quad \lambda_1 = \lambda_B - \lambda_A, \quad c(r) = c_A + c_1 s(r),$$
$$c_1 = c_B - c_A, \quad \rho(r) = \rho_A + \rho_1 s(r), \quad \rho_1 = \rho_B - c_A, \tag{3}$$

where $s(r)$ is the characteristic function of the region $s$ occupied by the fibers ($s(r) = 1$ if $r \in s$, $s(r) = 0$ if $r \notin s$).

From Eqs. (2) and (3), the governing equation of temperature in the REV can be obtained:

$$\lambda_A\nabla^2\vartheta(r) + i\rho_A c_A\omega\vartheta(r) = -\nabla\lambda_1\bar{t}(r)s(r) - i\omega\rho_1 c_1\vartheta(r)s(r), \tag{4}$$

Here $\bar{t}(r) = \nabla\vartheta(r)$.

Applying the operator $(\lambda_A\nabla^2 + i\rho_A c_A\omega)^{-1}$ to both sides of Eq. (4), we obtain the integral equation for the temperature field $\vartheta(r)$ in the form:

$$\vartheta(r) = \vartheta_A(r) + \int_{s_0}[\nabla G(r-r')\lambda_1\bar{t}(r') + i\omega G(r-r')\rho_1 c_1\vartheta(r')]s(r')\,dr', \tag{5}$$

where $\vartheta_A(r)$ is the temperature field that would have existed in the medium without fibers ($\lambda_1 = 0$, $c_1 = 0$, $\rho_1 = 0$). $G(r)$ is the Green function of the operator $\lambda_A\nabla^2 + i\rho_A c_A\omega$ [17], and is expressed as

$$G(r) = -\frac{i}{4\lambda_A}H_0^{(1)}(k_A|r|), \tag{6}$$

where $H_0(\cdot)$ is the Hankel function of the first kind and zero-order, $k_A$ is the complex wave number of thermal waves, and $k_A = (1+i)k$ with $k = \sqrt{\rho_A c_A\omega/2\lambda_A}$.

According to the hypotheses of EMM, the interaction between many fibers in the RVE can be reduced to a one-fiber problem. This problem is the diffraction of a monochromatic thermal wave on an isolated fiber embedded in the effective medium with the properties $\lambda_e$, $c_e$ and $\rho_e$. The effective thermal wave field is $\vartheta_e(r) = \bar{\vartheta}_e\, e^{i(\mathbf{k}_e\cdot r - \omega t)}$ with $\mathbf{k}_e = k_e\mathbf{n}$. Note that $k_e$ is the effective wave number.

Thus, the integral equation denoted by the effective field in the one-fiber region is described as

$$\vartheta(r) = \vartheta_e(r) + \int_{s_0}[\nabla G_e(r-r')\lambda_{e1}\bar{t}(r') + i\omega G_e(r-r')\rho_{e1}\vartheta(r')]\,dr', \tag{7}$$

Here $S_0$ is the area of the fiber cross-section, $G_e(r)$ is the Green function of effective medium, and $\lambda_{e1} = \lambda_B - \lambda_e$, $c_{e1} = c_B - c_e$, $\rho_{e1} = \rho_B - \rho_e$.

Let the general solution of Eq. (5) be known, and the temperature field $\vartheta(r)$ inside the fiber with the center at point $r^0 = 0$ be presented in the form:

$$\vartheta(r) = (\Lambda\vartheta_e)(r) = \Lambda[\bar{\vartheta}_e\, e^{i\mathbf{k}_e\cdot r}], \tag{8}$$

Here $\Lambda$ is a linear operator that depends on the dynamic properties of the effective medium and fiber.

If the fiber occupies area $S_0$ with the center at a point $r^0 \neq 0$, one can present the field $\vartheta(r)$ inside such an inclusion in the following form ($r \in s_0$)

$$\begin{aligned}\vartheta(r) &= \Lambda[\bar{\vartheta}_e\, e^{i\mathbf{k}_e\cdot(r-r^0)}\, e^{i\mathbf{k}_e\cdot r^0}] = \Lambda[e^{i\mathbf{k}_e\cdot(r-r^0)}]\bar{\vartheta}_e\, e^{i\mathbf{k}_e\cdot r^0}\\ &= \Lambda[e^{i\mathbf{k}_e\cdot(r-r^0)}]\, e^{-i\mathbf{k}_e\cdot(r-r^0)}\bar{\vartheta}_e\, e^{i\mathbf{k}_e\cdot r}\\ &= \Lambda^{\vartheta}(r-r^0)\vartheta_e(r),\ \Lambda^{\vartheta}(z) = \Lambda[e^{i\mathbf{k}_e\cdot z}]\, e^{-i\mathbf{k}_e\cdot z}.\end{aligned} \tag{9}$$

Similarly, from $\bar{t}(r) = \nabla\bar{\vartheta}(r)$, the following can be obtained:

$$\bar{t}(r) = \nabla\Lambda[\bar{\vartheta}_e\, e^{i\mathbf{k}_e\cdot(r-r^0)}\, e^{i\mathbf{k}_e\cdot r^0}] = \Lambda^\tau(r-r^0)\vartheta_e(r),$$
$$\Lambda^t(z) = \nabla\Lambda[e^{i\mathbf{k}_e\cdot z}]e^{i\mathbf{k}_e\cdot z}, \tag{10}$$

Note that $\Lambda^\vartheta(z)$ and $\Lambda^t(z)$ do not depend on the position $r=0$ of the center of the fiber. They can be constructed from the solution of the one-fiber problem for the fiber centered at the point $r=0$.

Let us introduce random functions $\chi^\vartheta(r)$ and $\chi^t(r)$ in 2D-space. These functions coincide with $\Lambda^\vartheta(r-r^i)$ and $\Lambda^t(r-r^i)$ if $r$ is inside the fiber centered at point $r^i (i=1, 2, 3, \ldots)$, and they are equal to zero in the matrix. Substitution of Eqs. (9) and (10) into Eq. (5) yields the following:

$$\vartheta(r) = \vartheta_A(r) + \int_{S_0}[\nabla G(r-r')\lambda_1\chi^t(r')\vartheta_e(r') + i\omega G(r-r')\rho_1 c_1\chi^\vartheta(r')\vartheta_e(r')]S(r')\,dr', \tag{11}$$

In order to find the mean wave field, let us average both sides of Eq. (11) over ensemble realization of the random set of fibers, and take into account the condition of $\vartheta_e(r) = \langle\vartheta(r)\rangle$, the following can be obtained:

$$\langle\vartheta(r)\rangle = \vartheta_A(r) + \phi(Y_0)\int[\nabla G(r-r')\lambda_1\Lambda^c + i\omega G(r-r')\rho_1 c_1\Lambda_\rho]\langle\vartheta(r')\rangle\,dr', \tag{12}$$

$$\Lambda_\rho(\mathbf{k}_e) = \lim_{\Omega\to\infty}\frac{1}{\phi(Y_0)\Omega}\int_\Omega\chi^\vartheta(r)\,dr = \frac{1}{\langle s\rangle}\left\langle\int_s\Lambda^\vartheta(r)\,dr\right\rangle, \tag{13}$$

$$\Lambda^c(\mathbf{k}_e) = \lim_{\Omega\to\infty}\frac{1}{\phi(Y_0)\Omega}\int_\Omega\chi^t(r)\,dr = \frac{1}{\langle s\rangle}\left\langle\int_s\Lambda^t(r)\,dr\right\rangle, \tag{14}$$

where $\Lambda_\rho$ and $\Lambda^c$ are constant scalar and vector, respectively, $\Omega$ is the two dimensional plane $(x,y)$ in the RVE, $\phi(Y_0)$ is the volume fraction at the material point $Y_0$, and $s$ is the area occupied by the typical fiber.

Let us apply the Fourier transform to Eq. (12) and multiply the result with $L_A(k) = \lambda_A k^2 - i\rho_A c_A\omega$. Taking into account the equations:

$$L_A(\mathbf{k})G(\mathbf{k}) = 1, \qquad L_A(\mathbf{k})\vartheta_A(\mathbf{k}) = 0, \tag{15}$$

the following can be obtained

$$L_e(\mathbf{k})\langle\vartheta(\mathbf{k})\rangle = 0,$$
$$L_e(\mathbf{k}) = L_A(\mathbf{k}) + \phi(Y_0)\lambda_1 ik_i\Lambda^c(\mathbf{k}_e) - \phi(Y_0)\rho_1 i\omega\Lambda_\rho(\mathbf{k}_e) - \phi(Y_0)c_1 i\omega\Lambda_\rho(\mathbf{k}_e). \tag{16}$$

Because vector $\Lambda^c$ in Eq. (15) is a function of the vector $\mathbf{k}_e$ only, $\Lambda^c$ may be written as

$$\Lambda^c(\mathbf{k}_e) = -ik_e H_C(k_e), \quad k_e = |\mathbf{k}_e| \tag{17}$$

where $H_C(k_e)$ is a scalar function. If the mean temperature field $\langle\vartheta(\mathbf{r})\rangle$ is a plane thermal wave ($\langle\vartheta(\mathbf{r})\rangle = \bar{\vartheta}_e\, e^{i\mathbf{k}_e\cdot r}$), its Fourier transform is $\langle\vartheta(\mathbf{k})\rangle = (2\pi)^{-1}\bar{\vartheta}_e\delta(\mathbf{k}-\mathbf{k}_e)$, and Eq. (15) takes the form $L_e(\mathbf{k})\delta(\mathbf{k}-\mathbf{k}_e) = 0$, namely:

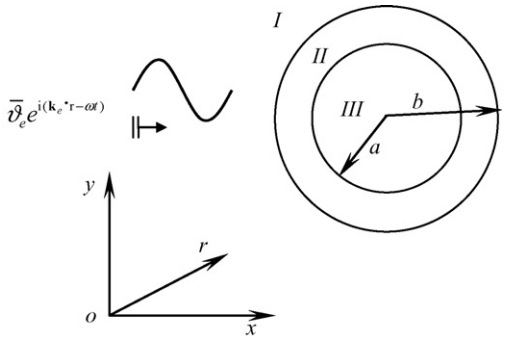


Fig. 2. Schematic of the wave fields in one-fiber problem.

$$L_e(\mathbf{k}_e) = L_A(\mathbf{k}_e) + \phi(Y_0)\lambda_1(k_e)^2 H_C(k_e) - \phi(Y_0)\rho_1 i\omega\Lambda_\rho(k_e) - \phi(Y_0)c_1 i\omega\Lambda_\rho(k_e) = 0. \tag{18}$$

This equation may be simplified as

$$\lambda_e(k_e)k_e^2 - i\omega[\rho_e(k_e) + c_e(k_e)] = 0,$$
$$\lambda_e(k_e) = \lambda_A + \phi(Y_0)\lambda_1 H_C(k_e),\ \rho_e(k_e) = \rho_A + \phi(Y_0)\rho_1\Lambda_\rho(k_e),$$
$$c_e(k_e) = c_A + \phi(Y_0)c_1\Lambda_\rho(k_e). \tag{19}$$

Note that Eq. (19) is the dispersion relation for the effective wave number $k_e$ of the mean thermal wave field in the RVE.

The one-fiber problem in the effective temperature field is shown in Fig. 2. Zone I denotes the effective field, zone II denotes the matrix, zone III denotes the fiber, and the radius of the fiber is $a (a \ll d_1)$. The relation between $a$ and $b$ is $(a/b)^2 = \phi(Y_0)$.

To obtain $H_C(k_e)$ and $\Lambda_\rho(k_e)$, the differential equations of the one-fiber problem are given by

$$\partial^2\vartheta + k_B^2\vartheta = 0, \quad |r| < a, \quad k_B^2 = \frac{i\rho_B c_B\omega}{\lambda_B}. \tag{20}$$

$$\partial^2\vartheta + k_A^2\vartheta = 0, \quad a < |r| < b, \quad k_A^2 = \frac{i\rho_A c_A\omega}{\lambda_A}. \tag{21}$$

$$\partial^2\vartheta + k_e^2\vartheta = 0, \quad b < |r|, \quad k_e^2 = \frac{i\rho_e c_e\omega}{\lambda_e}. \tag{22}$$

The solutions of them have the following forms:

$$\vartheta(r) = \sum_{m=0}^{\infty} a_m J_m(k_B r)\cos(m\varphi), \quad 0 \le r \le a. \tag{23}$$

$$\vartheta(r) = \sum_{m=0}^{\infty}[c_m J_m(k_A r) + d_m N_m(k_A r)]\cos(m\varphi), \quad a \le r \le b. \tag{24}$$

$$\vartheta(r) = \sum_{m=0}^{\infty}[\in_m(-i)^m\bar{\vartheta}_e J_m(k_e r) + b_m H_m(k_e r)] \times \cos(m\varphi), b < r. \tag{25}$$

where $N_m(\cdot)$ is the $m$th Bessel function of the second kind, $H_m(\cdot)$ is the $m$th Hankel function of the first kind, and $\in_m = 1$, if $m = 0$, $\in_m = 2$ if $m > 0$.

According to the continuous boundary conditions of the temperature and heat-flux density around the fiber, the mode coefficients take the following forms:

$$a_m = \frac{1}{\Delta}(B_1A_{22} - B_2A_{12}), \quad b_m = -\frac{1}{\Delta}(B_1A_{21} - B_2A_{11}),$$

$$c_m = \frac{\pi}{2\mu_0}A_{11}a_m, \quad \mathrm{d}_m = -\frac{\pi}{2\mu_0}A_{21}a_m,$$

$$\Delta = A_{11}A_{22} - A_{12}A_{21},$$

$$A_{11} = \lambda_\mathrm{A}k_\mathrm{A}aJ_m(k_\mathrm{B}a)N'_m(k_\mathrm{A}a) - \lambda_\mathrm{B}k_\mathrm{B}aJ'_m(k_\mathrm{B}a)N_m(k_\mathrm{A}a),$$

$$A_{12} = \lambda_\mathrm{e}k_\mathrm{e}bN_m(k_\mathrm{A}b)H'_m(k_\mathrm{e}b) - \lambda_\mathrm{A}k_\mathrm{A}bH_m(k_\mathrm{e}b)N'_m(k_\mathrm{A}b),$$

$$A_{22} = \lambda_\mathrm{e}k_\mathrm{e}bJ_m(k_\mathrm{A}b)H'_m(k_\mathrm{e}b) - \lambda_\mathrm{A}k_\mathrm{A}bH_m(k_\mathrm{e}b)J'_m(k_\mathrm{A}b),$$

$$B_1 = \in_m(-\mathrm{i})^m\bar{\vartheta}_\mathrm{e}[\lambda_\mathrm{A}k_\mathrm{A}bJ_m(k_\mathrm{e}b)N'_m(k_\mathrm{A}b) - \lambda_\mathrm{e}k_\mathrm{e}bJ'_m(k_\mathrm{e}b)N_m(k_\mathrm{A}b)],$$

$$B_2 = \in_m(-\mathrm{i})^m\bar{\vartheta}_\mathrm{e}[\lambda_\mathrm{A}k_\mathrm{A}bJ_m(k_\mathrm{e}b)J'_m(k_\mathrm{A}b) - \lambda_\mathrm{e}k_\mathrm{e}bJ'_m(k_\mathrm{e}b)J_m(kb)]. \quad (25)$$

Substituting Eq. (23) into Eqs. (13), (14) and (17), the following can be obtained:

$$\Lambda_\rho = \sum_{m=0}^{\infty}a_mg_m, \qquad H_\mathrm{C} = \sum_{m=0}^{\infty}a_mg_{1m}, \quad (26)$$

where

$$g_m = \frac{2i^m}{a}\frac{1}{k_\mathrm{B}^2 - k_\mathrm{e}^2}[k_\mathrm{B}J_{m+1}(k_\mathrm{B}a)J_m(k_\mathrm{e}a) - k_\mathrm{e}J_m(k_\mathrm{B}a)J_{m+1}(k_\mathrm{e}a)], \quad (27)$$

$$g_{1m} = g_m + \frac{2\mathrm{i}^m}{ak_\mathrm{e}}J_m(k_\mathrm{B}a)J'_m(k_\mathrm{e}a). \quad (28)$$

According to the dispersion relation in Eq. (19), we construct the numerical solutions of the effective properties. Based on Eq. (19), the numerical solutions are obtained by the iterative procedure, i.e.

$$\lambda_{1\mathrm{e}}^n = \lambda_{1\mathrm{e}}^{n-1} + \varepsilon[\lambda_{1\mathrm{e}}^{n-1} - \lambda_\mathrm{A}(1+\phi(Y_0)\bar{\lambda}_1H_\mathrm{C}(k_{1\mathrm{e}}^{n-1}, \lambda_{1\mathrm{e}}^{n-1}))],$$

$$\rho_{1\mathrm{e}}^n = \rho_{1\mathrm{e}}^{n-1} + \varepsilon[\rho_{1\mathrm{e}}^{n-1} - \rho_\mathrm{A}(1+\phi(Y_0)\bar{\rho}_1\Lambda_\rho(k_{1\mathrm{e}}^{n-1}, \rho_{1\mathrm{e}}^{n-1}))],$$

$$c_{1\mathrm{e}}^n = c_{1\mathrm{e}}^{n-1} + \varepsilon[c_{1\mathrm{e}}^{n-1} - c_\mathrm{A}(1+\phi(Y_0)\bar{c}_1\Lambda_\rho(k_{1\mathrm{e}}^{n-1}, c_{1\mathrm{e}}^{n-1}))],$$

$$k_{1\mathrm{e}}^n = (1+i)\left(\frac{\rho_{1\mathrm{e}}^nc_{1\mathrm{e}}^n\omega}{2\lambda_{1\mathrm{e}}^n}\right)^{1/2}, \quad \bar{\lambda}_1 = \frac{\lambda_1}{\lambda_\mathrm{A}},$$

$$\bar{\rho}_1 = \frac{\rho_1}{\rho_\mathrm{A}}, \quad \bar{c}_1 = \frac{c_1}{c_A}, \quad (29)$$

where $k_{1\mathrm{e}}^n, \lambda_{1\mathrm{e}}^n, c_{1\mathrm{e}}^n$ and $\rho_{1\mathrm{e}}^n$ are the effective parameters for the $n$th iteration, the subscript 1 denotes material zone 1, and functions $H_\mathrm{C}(k_{1\mathrm{e}},\lambda_{1\mathrm{e}})$, $\Lambda_\rho(k_{1\mathrm{e}},\rho_{1\mathrm{e}})$ and $\Lambda_\rho(k_{1\mathrm{e}},c_{1\mathrm{e}})$ are defined in Eq. (26). Parameter $\varepsilon(|\varepsilon| < 1)$ is to be chosen for conversion of the iterative process. As an initial (zero) approximation, the static solutions $k_{1\mathrm{e}}^{(0)} = (1+2\mathrm{i})\sqrt{[\rho_\mathrm{A} + \rho_1\phi(Y_0)][c_\mathrm{A} + c_1\phi(Y_0)]\omega/\lambda_{1\mathrm{s}}}$ and $\lambda_{1\mathrm{e}}^{(0)} = \lambda_{1\mathrm{s}}$ are applied. $\lambda_{1\mathrm{s}}$ is the static thermal conductivity, and is proposed as [8]

$$\lambda_{1\mathrm{s}} = \lambda_\mathrm{A}\left[1 + \frac{\alpha\phi(Y_0)[1+\phi(Y_0)\beta^2/4]+[1-\phi(Y_0)]}{\alpha\phi(Y_0)(\lambda_\mathrm{A}/\lambda_\mathrm{B})[1+\phi(Y_0)\beta^2/4]+[1-\phi(Y_0)]}\right], \quad (30)$$

Here $\alpha = 3\lambda_\mathrm{B}/(\lambda_\mathrm{B} + 2\lambda_\mathrm{A})$, $\beta = (\lambda_\mathrm{B} - \lambda_\mathrm{A})/(\lambda_\mathrm{B} + 2\lambda_\mathrm{A})$.

The dynamic effective thermal properties in the RVE correspond to those of the $Y_0$ layer in the global coordinate, so the dynamic effective properties in zone 1 ($0 \le Y \le d_1$) can be obtained by solving Eq. (29).

## 4. Solution of dynamic effective thermal properties in zones 2 and 3

According to the solving method in zone 1, the dynamic effective thermal properties in zone 3 ($d_2 \le Y \le d$) can be calculated by interchanging the fiber and matrix phases.

In transition zone 2 ($d_1 \le Y \le d_2$), the fiber and matrix phases cannot be well defined because the two phases may be interpenetrated into each other as a connected network. As a sequence, the effective wave fields of both phases cannot be explicitly determined by the above method. Following the work of Yin [6], a phenomenological transition function is introduced as

$$f(Y) = \left[1 - 2\frac{\phi(Y) - \phi(d_1)}{\phi(d_1) - \phi(d_2)}\right]\left[\frac{\phi(Y) - \phi(d_2)}{\phi(d_1) - \phi(d_2)}\right]^2, \quad (31)$$

so that the dynamic effective properties can be approximated as the combination of the solutions for two fiber–matrix zones, i.e.

$$\lambda_{2\mathrm{e}}(Y) = f(Y)\lambda_{1\mathrm{e}}(Y_0) + [1 - f(Y)]\lambda_{3\mathrm{e}}(Y_0). \quad (32)$$

$$\rho_{2\mathrm{e}}(Y) = f(Y)\rho_{1\mathrm{e}}(Y_0) + [1 - f(Y)]\rho_{3\mathrm{e}}(Y_0). \quad (33)$$

$$c_{2\mathrm{e}}(Y) = f(Y)c_{1\mathrm{e}}(Y_0) + [1 - f(Y)]c_{3\mathrm{e}}(Y_0). \quad (34)$$

Note that the subscripts 1, 2 and 3 denote the three material zones in Fig. 1.

## 5. Numerical examples and analysis

Consider a thermal wave propagating along the $Y$ direction in functionally graded materials, as shown in Fig. 1. For simplicity, it is assumed that $d = 1$. In zone 1 the reinforcing fibers are materials with high strength and good thermal conductivity, and the matrix consists of materials with high heat resistance. In zone 3, the fibers and matrix are interchanged. The following dimensionless variables and quantities have been chosen for computation: the wave number is $k^* = ka = 0.1$–$2.0$, the phase thermal conductivity contrast ratio is $\lambda^* = \lambda_\mathrm{B}/\lambda_\mathrm{A} = 5.0$–$20.0$, the phase specific heat capacity contrast ratio is $c^* = c_\mathrm{B}/c_\mathrm{A} = 2.0$–$5.0$, and the phase density contrast ratio is $\rho^* = \rho_\mathrm{B}/\rho_\mathrm{A} = 2.0$–$5.0$. According to Eqs. (29) and (32)–(34), the dynamic effective thermal conductivity, specific heat capacity and density in the overall thick of FGMs

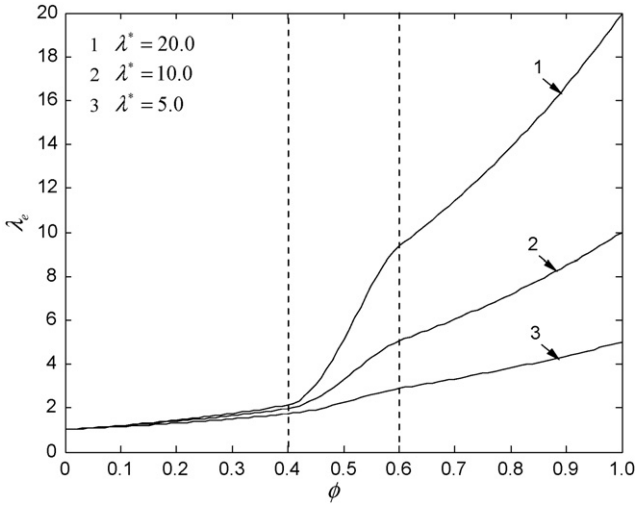


Fig. 3. Effect of phase thermal conductivity contrast ratio on effective thermal conductivity ($k^* = 0.01$, $c^* = 2.0$, $\rho^* = 2.0$, $m = 1.0$).

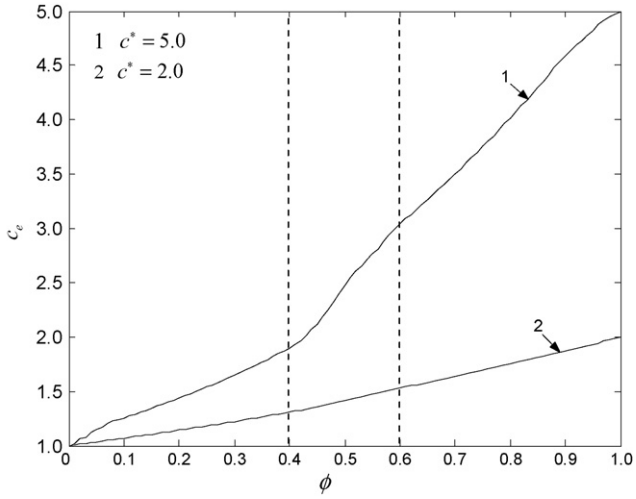


Fig. 4. Effect of phase specific heat capacity contrast ratio on effective specific heat capacity ($k^* = 0.01$, $\lambda^* = 10.0$, $\rho^* = 2.0$, $m = 1.0$).

can be obtained. It should be noted that we find that the truncation after $m = 12$ gives practically adequate results at any desired frequencies.

Following Bao and Cai's suggestion [18], the lower and upper bounds $d_1$ and $d_2$ are conveniently selected where the corresponding coordinates are $Y = 0.4$ and 0.6, respectively. The effect of phase thermal conductivity contrast ratio on the dynamic effective thermal conductivity in the gradation direction with parameters: $k^* = 0.01$ and $m = 1.0$ is illustrated in Fig. 3. It should be noted that when $k^* = 0.01$, the dynamic effective thermal conductivity tends to the static solution. It is found that the results in Fig. 3 are consistent with the static solutions in Ref. [6].

It can be seen from Fig. 3 that the dynamic effective thermal conductivity in the gradation direction of FGMs increases as the volume fraction of phase B increases, ranging from zone 1 (phase B as fiber phase) to zone 2 (transition zone) to zone 3 (phase B as matrix phase). Continuous and differentiable jump is expected in the transition zone when the phase thermal conductivity contrast ratio is relatively great. The greater the phase thermal conductivity contrast ratio, the greater the jump.

Shown in Fig. 4 is the effect of the phase specific heat capacity contrast ratio on the dynamic effective specific heat capacity in the gradation direction with parameters: $k^* = 0.01$ and $m = 1.0$. It can be seen that when the phase specific heat capacity contrast ratio is small, the effective specific heat capacity in the FGM gradation direction increases linearly as the volume fraction of phase B increases, ranging from zone 1(phase B as fiber phase) to zone 2 (transition zone) to zone 3 (phase B as matrix phase). However, when the phase specific heat capacity contrast ratio is great, continuous and differentiable jump is seen in the transition zone. The greater the phase specific heat capacity contrast ratio, the greater the jump.

Shown in Fig. 5 is the effect of the phase density contrast ratio on the dynamic effective density in the gradation direction with parameters: $k^* = 0.01$ and $m = 1.0$. It can be seen that the effective density in the FGM gradation direction increases linearly as the volume fraction of phase $B$ increases, ranging from zone 1(phase $B$ as fiber phase) to zone 2 (transition zone) to zone 3 (phase $B$ as matrix phase). Unlike the effective thermal conductivity and specific heat capacity, when the phase density contrast ratio is relatively great, the great jump of effective density exists in the three material zones. From Figs. 3–5, it is clear that when the variational function of $\phi(Y)$ is the same, the variation of effective thermal conductivity in the transition zone is the greatest, and the variation of effective density is the smallest.

The variation of dynamic effective thermal conductivity in the gradation direction under different frequencies of thermal waves is depicted in Fig. 6. It can be seen that as the incident wave number (frequency) increases, the effective thermal conductivity displays little variation in zone 1, while it shows great variation in zone 3. That is to say, the increase of incident frequency has great influence on the material zone with its matrix having good thermal conductivity, and the greater the wave frequency, the greater the influence. However, in the material zone with its fibers having good thermal conductivity, the effect of wave

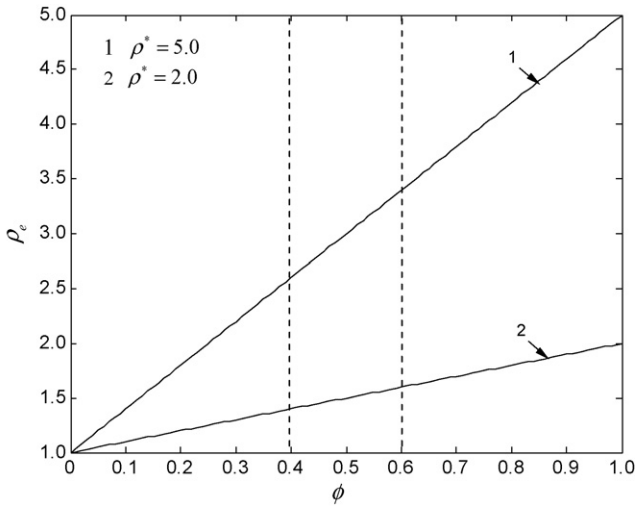


Fig. 5. Effect of phase density contrast ratio on effective density $k^* = 0.01$, $\lambda^* = 10.0$, $c^* = 2.0$, $m = 1.0$.

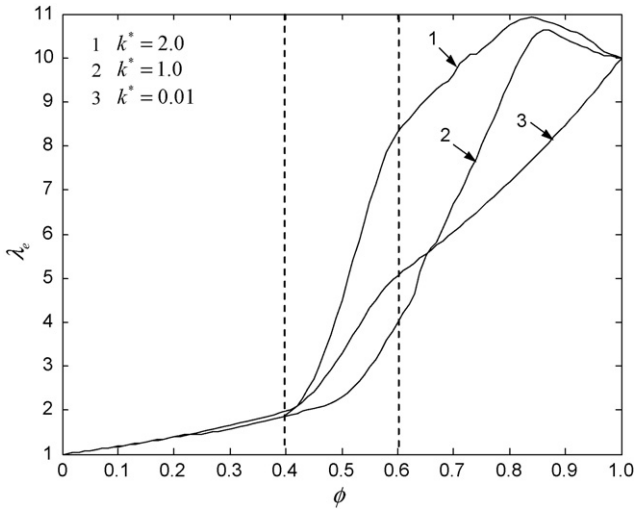


Fig. 6. Effect of wave number on effective thermal conductivity $\lambda^* = 10.0$, $c^* = 2.0$, $\rho^* = 2.0$, $m = 1.0$.

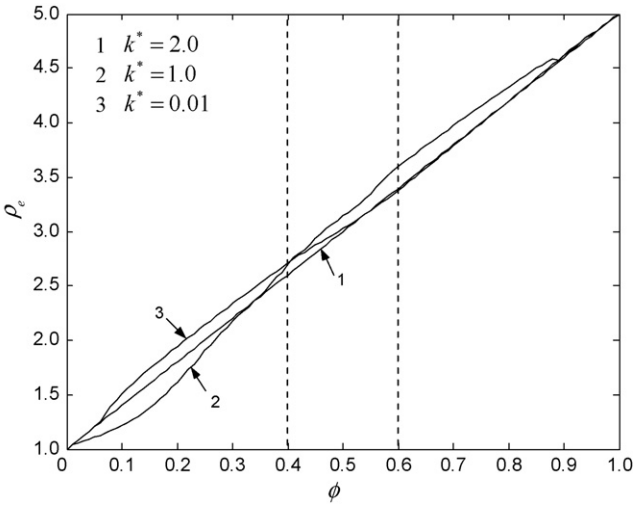


Fig. 8. Effect of wave number on effective density $\lambda^* = 10.0$, $c^* = 5.0$, $\rho^* = 5.0$, $m = 1.0$.

frequency on the dynamic effective thermal conductivity is little. As the incident wave number (frequency) increases, the variation of dynamic effective thermal conductivity in two fiber–matrix zones becomes little, while it has great jumps in transition zone. If the phase thermal conductivity contrast ratio is fixed, the jump of effective thermal conductivity in zone 2 increases with the increase of incident wave number.

Results for the effect of dimensionless wave number on the dynamic effective specific heat capacity in the gradation direction are presented in Fig. 7. It can be seen that as the incident wave number (frequency) increases, the effective specific heat capacity displays little variation in zone 1, while it shows great variation in zones 2 and 3. It is also clear that the effect of wave frequency on the effective specific heat capacity is similar to that on the effective thermal conductivity.

Results for the effect of dimensionless wave number on the dynamic effective density in the gradation direction are presented in Fig. 8. It can be seen that as the incident wave number (frequency) increases, the effective density displays little variation in the three zones. So, the thermal waves in materials have little effect on the effective density of FGMs. From Figs. 6–8, the effect of the wave frequency on the effective thermal conductivity in the gradation direction is the greatest, and the effect of the wave frequency on the effective density is the least.

Changing the phase volume fraction distribution also affects the dynamic thermal responses of FGMs. Fig. 9 illustrates the effect of gradation parameter on the distribution of dynamic effective thermal conductivity in the region of low frequency with four types of gradation parameter $m = 0.2$, 0.5, 1.5 and 3.0. It is clear that when $m > 1$, the greater the value of $m$, the greater the jump of the effective thermal conductivity in the transition zone. When $m < 1$, the less the value of $m$, the greater the jump of the effective thermal conductivity in the transition zone. In the case of $k^* = 1.0$, the distribution of dynamic effective thermal conductivity in the gradation direction with four types of gradation parameter is given in Fig. 10. From Figs. 9 and 10, it

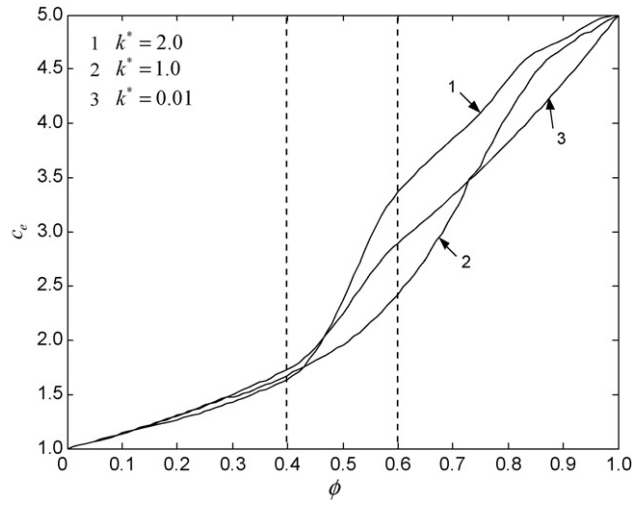


Fig. 7. Effect of wave number on effective specific heat capacity $\lambda^* = 10.0$, $c^* = 5.0$, $\rho^* = 5.0$, $m = 1.0$.

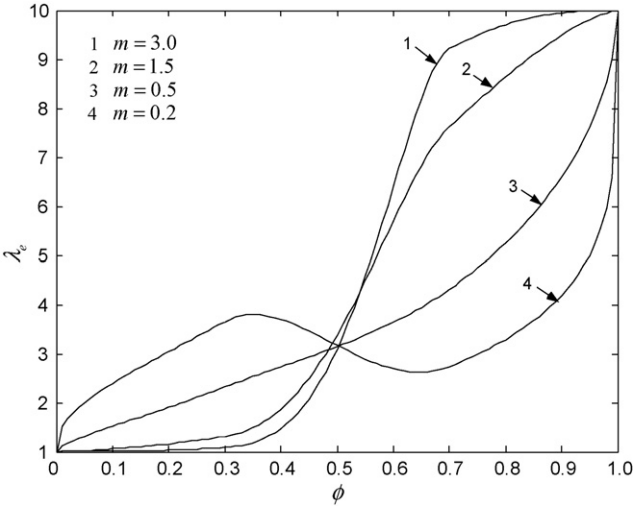


Fig. 9. Effect of gradation parameter on dynamic effective thermal conductivity $k^* = 0.1$, $\lambda^* = 10.0$, $c^* = 2.0$, $\rho^* = 2.0$.

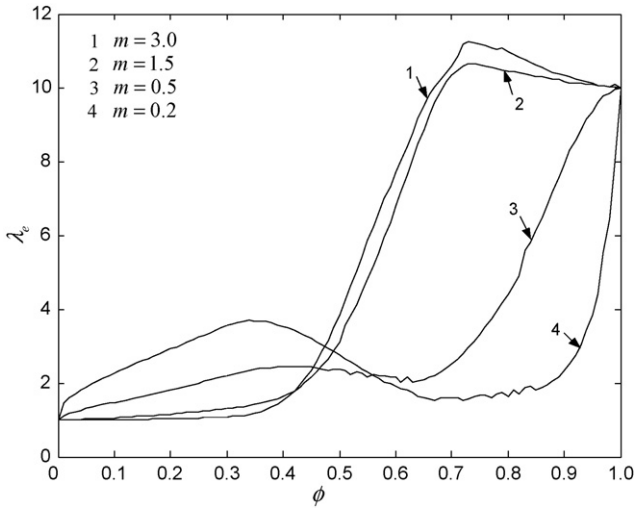


Fig. 10. Effect of gradation parameter on dynamic effective thermal conductivity $k^* = 1.0$, $\lambda^* = 10.0$, $c^* = 2.0$, $\rho^* = 2.0$.

can be seen that if $m > 1$ the variation of incident frequency has great effect on the distribution of dynamic effective thermal conductivity, and the greater the value of $m$, the greater the effect. However, in the case of $m < 1$ the increase of incident frequency has little effect on the distribution of dynamic effective thermal conductivity.

## 6. Conclusions

In this study, a micromechanics-based thermo-dynamical model is employed to analyze the dynamic effective thermal conductivity, specific heat capacity and density in the gradation direction of FGMs. The propagation of thermal waves along the gradation direction of FGMs is carried out. Comparisons with previous literatures demonstrate the validity of the micromechanics-based thermo-dynamical model.

During the course of derivation, three zones are divided in the thick of gradation direction, and in each zone the corresponding dynamic effective thermal properties are calculated. In fiber–matrix zones, a microscopic representative volume element is proposed to statistically represent the microstructure in the neighborhood of a material point and effective medium method is applied to derive the dynamic thermal effective properties. After obtaining the dispersion relation for effective wave number, the numerical solutions are given by iterative scheme. The numerical results show that the dynamic effective thermal properties in FGMs are significantly different from those in the static case. Therefore, to gain a better understanding of the microstructure–performance relationship and obtain the desirable material properties, it is important to analyze not only the static effective properties but also the dynamic effective properties.

Through analysis, it has been found that the dynamic effective thermal properties in the gradation direction are dependent on the incident wave number, the material properties of each phase, and the gradation parameter of FGMs. In the dynamic case, the effect of thermal wave frequency on the effect thermal conductivity in the gradation direction of FGMs is greater than that on the effective specific heat capacity. The effect of thermal wave frequency on the effect density in the gradation direction of FGMs is very little, and can be neglected. The increase of incident frequency has great influence on the material zone with its matrix having good thermal conductivity. To reduce the jump of effective properties in the transition zone, the phase properties contrast ratio should be considered. It is suggested that the larger transition zone made during FGMs fabrication is desirable to prevent the significant jump of the dynamic effective properties when the phase properties contrast ratio is large. In addition, in the gradation function $\phi(Y) = (Y/d)^m$, the value of $m$ should be restricted near 1.0, and the optimal value of it is $0.5 \leq m \leq 2.0$.

The analytical solutions presented in this paper may be useful for the optimizing design of the FGMs under dynamic thermal loading.

## Acknowledgement

The paper is supported by the National Natural Science Foundation of China (Foundation No. 10572045) and the Outstanding Youth Foundation of Hei Longjiang Province of China (Foundation No. JC-9). The authors are grateful to the anonymous reviewers for their constructive comments and suggestions.

## References

[1] L.J. Gray, T. Kaplan, J.D. Richardson, ASME J. Appl. Mech. 70 (2003) 543.
[2] H.-Y. Kuo, T. Chen, Int. J. Solids Struct. 42 (2005) 1111.
[3] K.A. KhorU, Y.W. Gu, Thin Solid Films 372 (2000) 104.
[4] M. Ostoja-Starzewski, J. Schulte, Phys. Rev. B 54 (1996) 278.
[5] H.M. Yin, L.Z. Sun, G.H. Paulino, Acta Mater. 52 (2004) 3535.
[6] H.M. Yin, G.H. Paulino, W.G. Buttlar, L.Z. Sun, J. Appl. Phys. 98 (2005), 063704.
[7] S.W. Gong, K.Y. Lam, J.N. Reddy, Int. J. Impact. Eng. 22 (1999) 397.
[8] L.L. Foldy, Phys. Rev. 67 (1945) 107.
[9] S.K. Bose, A.K. Mal, Int. J. Solids Struct. 9 (1973) 1075.
[10] H. Nozaki, Y. Shindo, Int. J. Eng. Sci. 36 (1998) 383.
[11] W. Liu, R.D. Kriz, Mech. Mater. 31 (1999) 117.
[12] A. Chakraborty, S. Gopalakrishnan, Int. J. Solids Struct. 40 (2003) 2421.
[13] A. Chakraborty, S. Gopalakrishnan, J.N. Reddy, Int. J. Mech. Sci. 45 (2003) 519.
[14] J.C. Nadeau, M. Ferrari, Compos. Eng. 5 (1995) 821.
[15] S.K. Kanaun, V.M. Levin, Int. J. Solids Struct. 40 (2003) 4859.
[16] Y.G. Gurevich, G.N. Logvinov, G.G. Cruz, G.E. Lopez, Int. J. Therm. Sci. 42 (2003) 63.
[17] A.C. Eringen, E.S. Suhubi, Elastodynamics, Academic Press, New York, London, 1974.
[18] G. Bao, H. Cai, Acta Mater. 45 (1997) 1055.